Effects of composition and magnetism on interfacial energy in Cu-Co alloys

Changle Li [1], Song Lu,[1,*] Wei Li,[2] Qing Chen [3] and Levente Vitos[1,2,4]

[1]*Applied Materials Physics, Department of Materials Science and Engineering,*
KTH Royal Institute of Technology, SE-10044 Stockholm, Sweden
[2]*Department of Physics and Astronomy, Division of Materials Theory, Uppsala University, Box 516, SE-75120 Uppsala, Sweden*
[3]*Thermo-Calc Software AB, Råsundavägen 18, SE-16967 Solna, Sweden*
[4]*Research Institute for Solid State Physics and Optics, Wigner Research Center for Physics, P.O. Box 49, H-1525 Budapest, Hungary*

The composition and magnetic dependent interfacial energy in Cu-Co immiscible alloys is investigated within a coherent interface model using *ab initio* calculations. We translate the composition dependence of the interfacial energy to the temperature dependence considering the variations of the equilibrium compositions of precipitate and matrix with respect to temperature. The obtained results are in reasonable agreement with those obtained by experiments and thermodynamic calculations. Reviewing the experimental methods for determining the interfacial energy based on kinetic models for precipitate nucleation and coarsening, as well the thermodynamic models based on broken-bond models, we point out that the temperature effect on the interfacial energy in the above models is primarily due to the composition change of the interface. The present work emphasizes the effort to understand the meaning of the speciously same quantity in different methods.

I. INTRODUCTION

Immiscible alloys, like Cu-Co, Cu-Fe, Cu-Cr, Cu-W, etc., exhibiting a miscibility gap, usually have complex thermodynamic properties when phase separation occurs during the actual solidification process [1–3]. Among them, Cu-Co alloys, an important system finding applications as magnetoresistance materials [4], have been extensively studied. This is one of the most famous systems for studying precipitation process from a supersaturated solid solution and for investigating precipitation hardening effects. The phase diagram of a Cu-Co binary system [5] shows virtually no solubility of Co in Cu or Cu in Co below 800 K. Upon annealing of supersaturated Cu-rich alloys, Co-rich precipitates of face-centered cubic (fcc) structure form within the Cu-rich matrix, or vice versa. This system is further complicated by the existence of magnetic transition and martensitic phase transformation in the Co-rich phase with varying temperature. The precipitate morphology and the characteristics of the precipitate/matrix interface also change with increasing precipitate size [6,7]. Extensive experimental measurements on the kinetics of Co precipitation from dilute Cu-Co alloys exist with the aim to study various kinetic models, including the theory of Lifshitz and Slyozov [8] and Wagner [9] (LSW) and diverse extended LSW models [10–15]. The interfacial energy (γ) obtained

from these studies depends significantly on the chosen kinetic model and the thermodynamic parameters. For example, Ardell and Nicholson [16] estimated $\gamma \approx 0.30$–1.00 J/m^2 within temperatures between 823 and 873 K in Cu-Co alloys based on Livingston's data of precipitate sizes using the original LSW theory [17]. Later, Ardell [10] proposed a modified theory taking into account the volume fraction of precipitate and reported significantly smaller values ($\gamma \approx 0.15$–0.32 J/m^2) based on the same set of coarsening data. The revised interfacial energies have a good agreement with the value of 0.19 J/m^2 reported by Servi *et al.* [18]. Recently, Watanabe *et al.* investigated the precipitate growth kinetics in Cu-Co [7,19], Cu-Fe [20], and Cu-Co-Fe [21] alloys, and the derived interfacial energy in Cu-Co alloys was $\sim$0.14–0.16 J/m^2 for temperatures between 823 and 973 K. In a Cu-1at. % Co alloy, Hattenhauer and Hassen reported an interfacial energy of 0.24 J/m^2 using a modified Langer-Schwartz theory [12].

Despite of the large uncertainty associated with experimental interfacial energy values as observed for the case of Cu-Co alloys, for a lot of systems, experimental interfacial energies are not available, not to mention the temperature or composition dependence. Alternatively, interfacial energies may be estimated by various thermodynamic models using the input data from CALPHAD-type thermodynamic databases via the approaches based on the nearest-neighbor broken bond (NNBB) [22,23]. Such approaches formulate the interfacial energy in a single, closed equation, which can give a fast estimation with varying composition and temperature. This is a critical requirement for computational modeling of precipitation nucleation and coarsening, e.g., in tools like TC-PRISMA [24–26], however, the accuracy of those data should be assessed carefully. For many cases, the interfacial energy needs to be treated as an adjustable parameter in the way

---

*songlu@kth.se

that the modeling results fit experiments. Besides the NNBB model, Kaptay [27] developed an alternative thermodynamic model for the coherent interfacial energy using the molar Gibbs energy and the molar volume as the initial data.

First-principles methods based on density functional theory (DFT) [28,29] are expected to be reliable for determining the interfacial properties because of the accurate representation of the atomic-scale physics both in bulk and around the planar faults. Calculations for coherent interfaces have been performed for various interfaces, including metal/ceramic [30] and metal/metal [31–33] interfaces. *Ab initio* interfacial studies are however normally limited to the chemically and structurally sharp interface at the temperature of 0 K. Few studies extended *ab initio* studies to interfaces with a diffusional chemical profile or varying temperature-dependent compositions. This situation limits a direct comparison between *ab initio* results and those from thermodynamic models and experiments. There have been a few attempts to include temperature effects on the interfacial energy, i.e., by including electronic and vibrational entropy contributions for a coherent interface [34]. Such studies are extremely expensive and only limited to very few wspecial cases such as the Ni/Ni$_3$Al interface with fixed compositions. No chemical variations on both sides of the interface were considered. Thus, one may see that even though it is desirable to use *ab initio* interfacial energies in thermodynamic and kinetic models to improve their power of prediction by placing the models on more solid basis of physics, such effort is hindered by a lack of comprehensive understanding of the difference in the quantity of the interfacial energy obtained by different methods.

The purpose of the present work is to explore the composition and temperature dependent interfacial energy using the first-principles calculations. In the model Cu-Co alloys, composition and magnetism dependent interfacial energy for the coherent interface is studied, which allows us to discuss the temperature dependence of the interfacial energy and compare to the thermodynamic and experimental results. We emphasize that such an effort to improve the understanding in the quantity of the interfacial energy from various methods and models is crucial for improving the transferability of this parameter between different methods.

II. METHODOLOGY

A. Interfacial energy

Interfacial energy may be separated into chemical ($\gamma^{\text{chem.}}$) and elastic ($\gamma^{\text{str.}}$) contributions, respectively. Our first step is to compute $\gamma^{\text{chem.}}$ for a chemically sharp interface. A supercell composed of equal numbers of atomic layers (N) of the Cu-rich A (Cu$_{1-x}$Co$_x$) and Co-rich B (Cu$_x$Co$_{1-x}$) phases was employed. Since the phase diagram shows that at the equilibrium state the compositions of the precipitate and the matrix are almost symmetric, so in the present work, only Cu$_{1-x}$Co$_x$/Co$_{1-x}$Cu$_x$ interfaces are considered. For the coherent interface, each layer has one lattice site occupied randomly by Cu and Co atoms. To reach coherency at the interface, we considered two cases using the equilibrium fcc Co-rich or Cu-rich lattices as the underlying lattice, respectively, as

(a) Top view **(b) Front view**

Origin

Case I

$a_{111} = a_{\text{Cu-rich}}$

Case II

$a_{111} = a_{\text{Co-rich}}$

d_i

[1 -1 0]
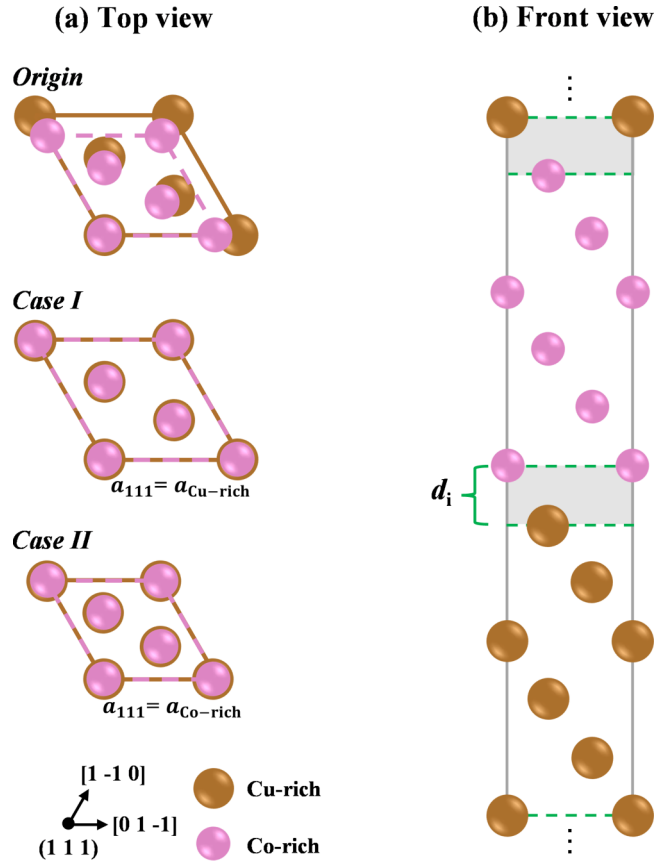[0 1 -1]
(1 1 1)

● Cu-rich
● Co-rich

FIG. 1. Schematic of the coherent interface composed of (111) atomic layers taking the Cu-rich (case I) or the Co-rich (case II) phases as the underlying lattice, respectively. In constrained relaxation calculations, the interface distance (d_i) was relaxed and the distorted lattice was assumed to keep the ideal c/a value $\sqrt{6}/3$.

shown in Fig. 1(a). For example, when the interface supercell takes Cu lattice parameters, the Co lattice is expanded accordingly, while keeping the symmetry of the fcc lattice, i.e., c/a keeps the ideal value. The interface distance (d_i) between the Cu-rich and Co-rich lattices was relaxed. To assess the error associated with the above constrained relaxation mode, atomic relaxation for all atoms was also performed in VASP calculations. In EMTO calculations, only the constrained relaxation method was adopted, though measuring the total energy changes with respect to d_i. The VASP and EMTO calculated interfacial energies are listed in Table I. Despite that full relaxation leads to lower interfacial energies, when only interfacial layer relaxation is considered, the convergence of the interfacial energy with respect to supercell size is much more stable and faster. The convergence is particularly problematic when the Co-rich lattice is distorted where magnetism can cause difficulties in convergence. Thereby, in the following studies, the constrained relaxation scheme is adopted for all calculations.

The chemical interfacial energy $\gamma^{\text{chem.}}$ for a model A/B interface is defined as

$$\gamma^{\text{chem.}} = \frac{E_{A/B}(x) - NE_A(x) - NE_B(x)}{2S}, \quad (1)$$

TABLE I. The (111) interfacial energy (in J/m^2) computed by EMTO and VASP for the Cu/Co interface with respect to the number of layers N. For comparison, the fully relaxed results (VASP-fr) along the normal direction of the interface are also listed.

		$N = 6$	$N = 9$	$N = 12$	$N = 15$
Case I	EMTO	0.264	0.264	0.280	0.264
	VASP	0.282	0.282	0.288	0.294
	VASP-fr	0.206	0.206	0.245	0.233
Case II	EMTO	0.245	0.245	0.263	0.261
	VASP	0.237	0.237	0.265	0.253
	VASP-fr	0.195	0.195	0.221	0.210

where $E_{A/B}(x)$ is the total energy of the supercell with two interfaces, $E_A(x)$ and $E_B(x)$ are the reference bulk energies (per layer) of the A and B phases under the same strain state as in the corresponding interface supercell, S is the area of the interface. The reference energies are calculated using an incremental method, e.g., from the total energy difference between the interface supercells with $N = 9$ and $N = 6$. The convergence test results are summarized in Table I. The strain energy contribution to the total coherent interfacial energy may be evaluated from the energy difference between the distorted and equilibrium lattices. When taking A as the underlying lattice,

$$\gamma^{\text{str.}} = \frac{E_B^{\text{str.}}(x) - E_B^{\text{eq.}}(x)}{S}, \tag{2}$$

where $E_B^{\text{eq.}}(x)$ is the total energy (per layer) of the B phase at the equilibrium state. Since strain energy contribution is volume dependent, here only one interface layer is considered, which is consistent with the interfacial energy calculation using thermodynamic method based on the NNBB model [35]. However, we must notice that in some studies, the strain energy was calculated for the whole precipitate or contained only the contribution from lateral strains [36,37]. Further studies are needed to decide which is the case closer to the real situation.

B. Computational details

All total energy calculations were performed using DFT in combination with the exact muffin-tin orbitals (EMTO) method [38–40], Green function, and the full charge density techniques. The self-consistent calculations were carried out with the local-density approximation (LDA) by Perdew and Wang [41] and the total energies were calculated with revised Perdew, Burke, and Ernzerhof exchange-correlation functional for solids (PBEsol) [42] via the full charge density technique [43,44]. The above non-self-consistent approach has the accuracy of the fully self-consistent calculations but is more efficient for very open systems, like free surfaces [45–47]. We adopted the coherent potential approximation (CPA) [48] to describe the compositional disorder. For the bulk calculations, a k-point mesh of $13 \times 13 \times 13$ was employed in the irreducible Brillouin zone. The convergence of the interfacial energy was carefully tested with respect to

the k-point mesh and we found that $15 \times 29 \times 1$ k points can reach a convergence within approximately 1% error.

The Co-rich phase was treated at the ferromagnetic (FM) state due to its high magnetic transition temperature. For the Cu-rich phases, three kinds of magnetic states were considered: FM and paramagnetic (PM) for temperatures lower and higher than Curie temperature (T_C), respectively, and a mixed one (PM+FM) corresponding to the case when the FM Co-rich slab induces magnetic polarization within a limited depth in the otherwise PM Cu-rich side across the chemical interface. We notice that in a fully self-consistent floating spin study of the PM Cu$_{0.9}$Co$_{0.1}$/FM Cu$_{0.1}$Co$_{0.9}$ interface, the first interface layer on the Cu-rich side becomes FM. The critical temperatures for the specific magnetic interfaces described above were estimated from the corresponding total energies. For the Cu-Co alloy system, in our previous study [5] we computed the critical temperatures using the mean-field approximation via $3k_B T_C = 2(E^{\text{PM}} - E^{\text{FM}})/(1 - c)$, where E^{PM} and E^{FM} are the energies of the PM and FM states, respectively, and c is the concentration of the nonmagnetic element (Cu). Our results showed a good agreement with the available experimental and theoretical values, despite the slightly overestimation, which is a common problem of this approach [49]. In the present case we computed the total energies of the different magnetic configurations for the Cu$_{0.9}$Co$_{0.1}$/Cu$_{0.1}$Co$_{0.9}$ interface system described by a supercell consisting of nine Cu-rich and nine Co-rich layers ($N = 9$). From the energy obtained for the FM/FM, PM+FM/FM, PM/FM, and PM/PM configurations, we found that the FM Cu-rich/FM Co-rich coherent interface is stable up to ∼200 K, the PM+FM Cu-rich/FM Co-rich interface is stable between ∼200 and ∼400 K, the full Cu-rich side becomes PM above ∼400 K, and both the Cu-rich and Co-rich sides turn PM above ∼1100 K [50]. We notice that with increasing cell size, the above critical temperatures are expected to converge towards the bulk values presented in Ref. [5]. According to the above critical temperatures, the present DFT calculations for the interfaces were performed for the three magnetic configurations (FM/FM, PM+FM/FM, and PM/FM) describing the situation below the Curie temperature of Co. In addition, for comparison we also present results for the full PM (PM-Cu/PM-Co) interface. Similar magnetic interaction at the interface was observed in the Fe-Cr α/α' phase interfaces [31]. In all cases, the PM state was described by the disordered local magnetic moment (DLM) scheme [51] in combination with CPA, i.e., equal concentrations of Co atoms with up and down collinear spins on each atomic sites are considered [e.g., the Cu$_{1-x}$Co$_x$ layer was described as a Cu$_{1-x}$(Co$_{0.5}^{\uparrow}$Co$_{0.5}^{\downarrow}$)$_x$ ternary alloy], to simulate the vanishing magnetization and nonzero local moments.

To evaluate our EMTO results, for example, for the purpose to assess the effect of relaxation, calculations by the Vienna *ab initio* simulation package (VASP) [29] using the projector augmented wave (PAW) method [52] were also performed. For the exchange-correlation functional we adopted the generalized gradient approximation parametrized by the Perdew, Burke, and Ernzerhof for solids (PBEsol). k-point meshes kept the same as the EMTO calculations. Cutoff energies were set to 500 eV for all calculations. The convergence criteria for

TABLE II. Structural parameters of the $Cu_{1-x}Co_x/Cu_xCo_{1-x}$ coherent interfaces. a^0 is the equilibrium lattice constants of the underlying lattice. a^0_{111} is the corresponding lattice parameters of the (111) plane, viz., $a^0_{111} = a^0/\sqrt{2}$. d_i is the optimized interface spacing. All parameters in the table are computed at the FM state.

	Underlying	a^0 (Å)	d_i/a^0_{111}
Case I	Pure Cu	3.571	0.816
	$Cu_{0.9}Co_{0.1}$	3.560	0.815
	$Cu_{0.8}Co_{0.2}$	3.550	0.815
	$Cu_{0.7}Co_{0.3}$	3.540	0.814
	$Cu_{0.6}Co_{0.4}$	3.529	0.815
Case II	$Cu_{0.4}Co_{0.6}$	3.510	0.818
	$Cu_{0.3}Co_{0.7}$	3.500	0.821
	$Cu_{0.2}Co_{0.8}$	3.491	0.825
	$Cu_{0.1}Co_{0.9}$	3.483	0.827
	Pure Co	3.475	0.832

electronic energy and force calculations were 10^{-5} eV and 0.02 eV/Å, respectively. As discussed above, we considered two kinds of relaxation in VASP calculations at the Cu/Co interface for comparison, (i) only interface relaxation (similarly in EMTO calculations); and (ii) full atomic relaxation. The comparison between EMTO and VASP results is summarized in Table I.

III. RESULTS

A. Structural parameters

The calculated lattice constants for fcc-Cu and fcc-Co are 3.57 and 3.47 Å, which are slightly smaller than those by using the PBE exchange-correlation functional (e.g., 3.64 Å for fcc-Cu [5] and 3.53 Å for fcc-Co [5]). This is consistent with previous calculations [47,53]. Nevertheless, the PBEsol results agree better with the room-temperature experimental data (3.61 Å for fcc-Cu [4] and 3.55 Å for fcc-Co [4]). The composition dependent lattice parameters of Cu-Co alloys are listed in Table II, which agrees well with the trend from previous theoretical calculations [5,54]. When taking the Cu-rich underlying lattice, the interface spacing is close to the ideal value ∼0.816. When taking the Co-rich underlying lattice, d_i/a^0_{111} are larger than the ideal one. Compared to the Co-rich underlying lattice, the variation of d for the Cu-rich underlying lattice is more moderate. The above observation is related to the different elastic moduli of the Cu-rich and Co-rich phases.

B. Composition-dependent interfacial energy

Figure 2 presents the calculated interfacial energy versus composition (x) for cases I and II for the FM/FM interface. For the case when only the interface layer distance is relaxed, both EMTO and VASP results agree well with each other. The chemical interfacial energy of the coherent Cu/Co interface is between ∼0.24 and ∼0.29 J/m², which is in line with the usual interfacial energies for coherent interfaces [55]. Full relaxation (VASP results) slightly decreases the interfacial energies for both cases I and II, as expected. The overall trend is that the interfacial energy
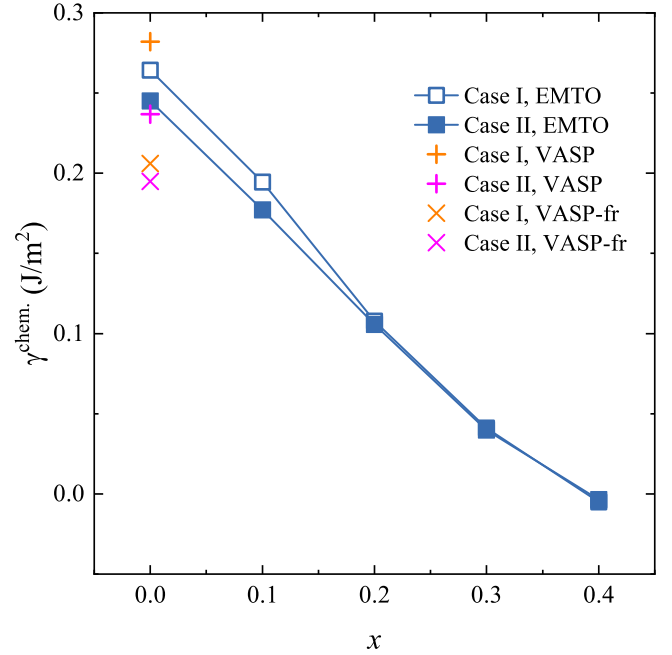

FIG. 2. The calculated coherent interfacial energy γ (in J/m²) for the $Cu_{1-x}Co_x/Cu_xCo_{1-x}$ symmetric interface as a function of composition x. Case I (open symbols) and case II (solid symbols) represent the interfaces taking Cu-rich (Co-rich) as the underlying lattice, respectively. All results correspond to the FM/FM interface. Two sets of VASP results from Table I for the pure Cu/pure Co interface are also included for comparison.

decreases monotonically with increasing x, i.e., when the chemical difference between the two phases is getting smaller. We notice that the chemical interfacial energy vanishes at $x \approx 0.4$ and becomes negative for even larger x. The interfacial energy for $Cu_{0.5}Co_{0.5}/Co_{0.5}Cu_{0.5}$ ($x = 0.5$) is calculated to be -0.018 J/m², which should obviously be 0. The deviation is ascribed to the incremental method for calculating the reference bulk energy and the numerical errors from factors like k-points sampling. Therefore, an underestimation of ∼0.02 J/m² should be expected for other interfaces too. Despite at the equilibrium state, the mutual solubility is very low even at high temperatures, supersaturated solid solution up to 26 at. % Co in Cu-Co alloys can be obtained at the as-deformed state by processing method like high-pressure torsion [14]. Annealing leads to further variations in the concentrations of the Cu-rich and Co-rich regions. The very small (even negative) interfacial energy for high-concentrated interfaces may be important for understanding the observed high thermal stability of nanocrystalline Cu-Co alloys [14].

This trend is interesting since the Co-rich underlying lattice has a smaller in-plane lattice parameter and a smaller interlayer distance compared to the Cu-rich underlying lattice case. We speculate that the lower excess energy in the Co-rich underlying lattice is associated with the total energies of the subsystem. Namely, in the Co-rich underlying lattice case, the fcc Cu part of the interface is distorted in order to match the fcc Co surface. Since Cu has a relatively small bulk modulus, the energy change with this lattice deformation is smaller than the one when the fcc Co is stretched to match the Cu
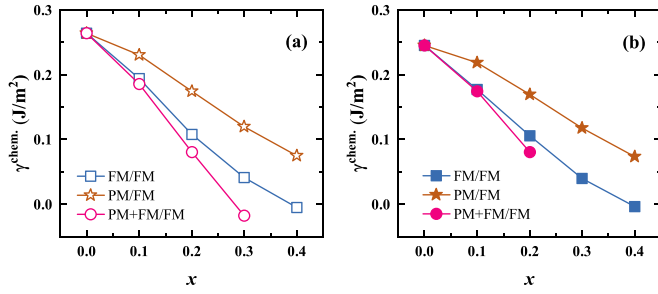
FIG. 3. Magnetic effects on the interfacial energy for the FM/FM (squares), PM/FM (stars), and PM+FM/FM (circles) interfaces. (a) and (b) The interfaces taking the Cu-rich (case I) and the Co-rich (case II) phases as the underlying lattice, respectively.

surface (Cu-rich underlying case). Smaller deformation energy decreases the energy of the entire system and thus leads to lower excess energy near the interface.

C. Magnetic effect on the interfacial energy

The effects of magnetism on the chemical interfacial energy are presented in Fig. 3. The Co-rich side is always in the FM state due to the high Curie temperature [5]. When comparing the results for the FM/FM and PM/FM interfaces, magnetism shows clear effects. The FM/FM interface leads to a lower interfacial energy. However, calculations showed that the interface layer on the PM Cu-rich side is often magnetized, i.e., becoming the PM+FM/FM state, which results in even lower interfacial energy than the FM/FM state (Fig. 3).

The strong decrease in the interfacial energy is related to the decrease of the total energy of the interface supercell, as well as to the choice of the reference state. For the calculation of the PM+FM/FM interfacial energy, the referenced bulk energy is obtained from the total energy difference between the 9+9 and 6+6 PM/FM supercells. Therefore, even for the FM spin polarized interface layer, the present interfacial energy is defined with respect to the PM bulk state. Since for the bulk Cu-rich alloy, the internal energy calculated at the FM state is lower than that at the PM state, it is easy to expect that when the PM bulk energy is chosen as the reference for the FM interface layer, the interfacial energy is decreased. Cases I and II show some deviations at small x, and become the same at large x. We would like to add that the sizable negative interfacial energy obtained for $x \geqslant 0.3$ [PM+FM/FM case in Fig. 3(a)], is due to the particular reference state (PM Cu-rich bulk) and to the fact that all these interfacial energies are computed from the internal energy not taking into account any thermomagnetic terms. However, as we will see in Sec. IV, the PM+FM/FM case is relevant only for very small x values (where the mutual solubility of Cu and Co is very low) and where in fact all Cu-rich layers are paramagnetic (nonmagnetic).

Figure 4 shows the calculated magnetic moments of the atoms in the $Cu_{1-x}Co_x/Cu_xCo_{1-x}$ interface with $x = 0.1$ and $x = 0.2$ at various magnetic states. Changing x results in very similar magnetic structure, only the sizes of the magnetic moments are slightly altered. For the FM/FM interfaces, on average, the Co atoms are slightly less magnetized at the Cu-rich side than those at the Co-rich side. Particularly, on
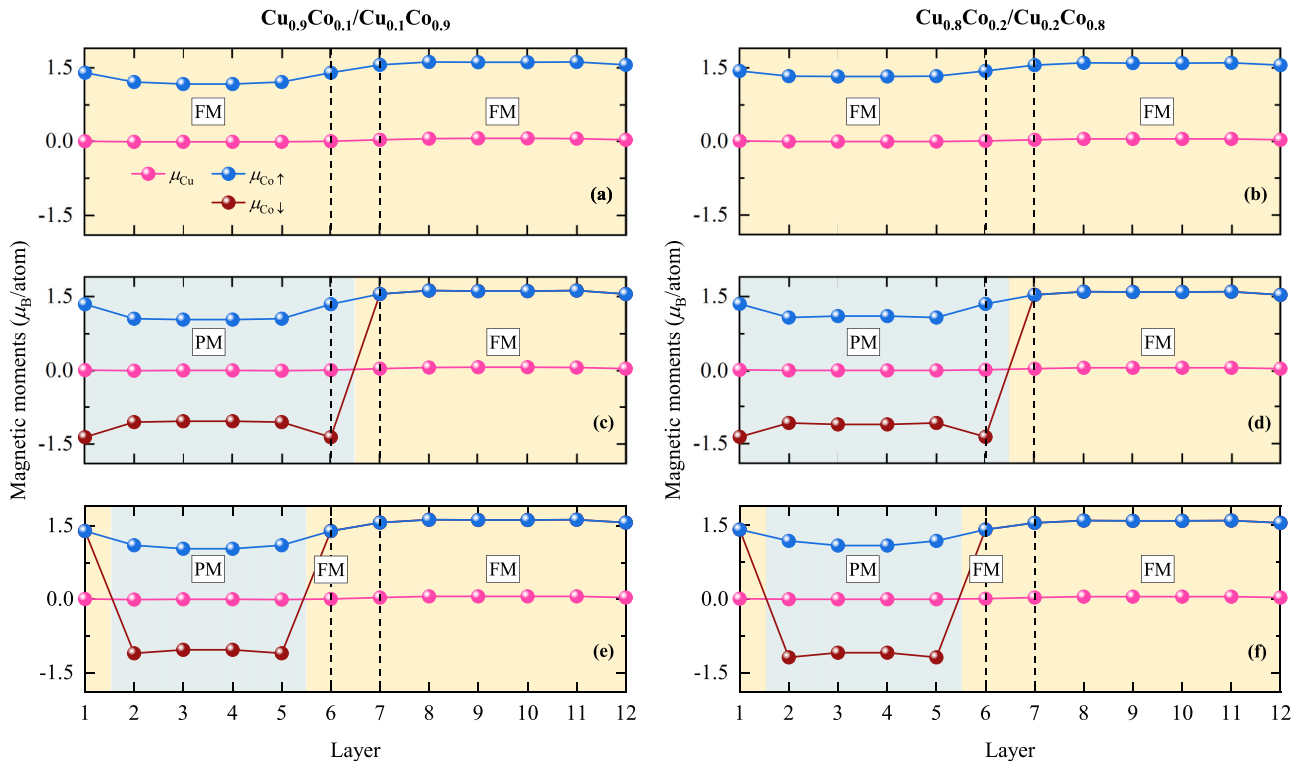

FIG. 4. The calculated magnetic moments (in μ_B/atom) of the atoms in case I for $x = 0.1$ and $x = 0.2$ for various magnetic interfaces. Atomic layers 1–6 belong to the Cu-rich phase and 7–12 to the Co-rich phase. Blue and yellow regions mark the PM and FM states, respectively.

the Cu-rich side, the magnetic moments of the interface Co atoms [layers 1 and 6 in Figs. 4(a) and 4(b)] are larger than those in the bulk (layers 2–5). While on the Co-rich side, the Co magnetic moments slightly decrease near the interface. For the PM/FM interface state, the absolute values of the Co magnetic moments have a similar trend as those at the FM/FM state, although the local magnetic moments are somewhat smaller. Because of the DLM approximation for the PM state, the local spin-up and spin-down moments of Co atoms are exactly the same, which gives the vanished total magnetization on the Cu-rich side. For the PM+FM/FM interfaces, the interface layers [layers 1 and 6 in Fig. 4(e) and 4(f)] in the PM Cu-rich side become ferromagnetically coupled to the Co-rich side. This leads to the increase of the local magnetic moments (in absolute value) for the Co atoms in layers 2 and 5, compared to the bulk magnetic moments in PM state [Figs. 4(c) and 4(d)].

The magnetic interaction between interfacial and subinterfacial atoms, as well as the effect on the interfacial energy, can be more clearly seen when we perform fixed-spin calculations (noticing that the magnetic moments on the bulk atoms are barely effected). For this purpose we performed floating-spin and constrained-spin calculations for the PM+FM $Cu_{0.7}Co_{0.3}$/FM $Cu_{0.3}Co_{0.7}$ interface. In the floating-spin calculations, where all the atomic magnetic moments are allowed to relax freely, the interfacial energy is -0.02 J/m^2 and the magnetic moment of the atom in the subinterface layers is 1.22 μ_B. The negative energy follows the general trend found in Fig. 3. Then in the constrained-spin calculations, we fix the local magnetic moments in layers 2 and 5 to a value between 0 and 1.5 μ_B, and allow the local moments in all other layers to relax freely. In this way we can monitor how magnetic moments interact between layers. The results are shown in Fig. 5. The calculated interfacial energies as a function of the size of the fixed spin follow a polynomial trend, which practically corresponds to the energy versus magnetization curve as described by the Landau theory [56] (Fig. 5, lower panel). The polynomial expression for the interfacial energy versus magnetic moment suggests a critical point at around $m = 1.15$ μ_B, which is in good agreement with the fully relaxed result ($m = 1.22$ μ_B).

IV. DISCUSSION

In the following we briefly review the primary experimental methods for determining the interfacial energy for precipitate in alloys and the broken-bond models adopted by thermodynamical calculations for assessing the interfacial energy. We will show that in these methods the calculated interfacial energies at various temperatures correspond to the temperature-dependent compositions of the interface. Then we translate the composition and magnetic dependence of the interfacial energy to the temperature dependence. Reasonable agreement with available results in literature is reached.

A. Experimental interfacial energy in Cu-Co alloys

As mentioned in the Introduction, no direct method is available for measuring the interfacial energy. The commonly referred "experimental interfacial energies" are derived from
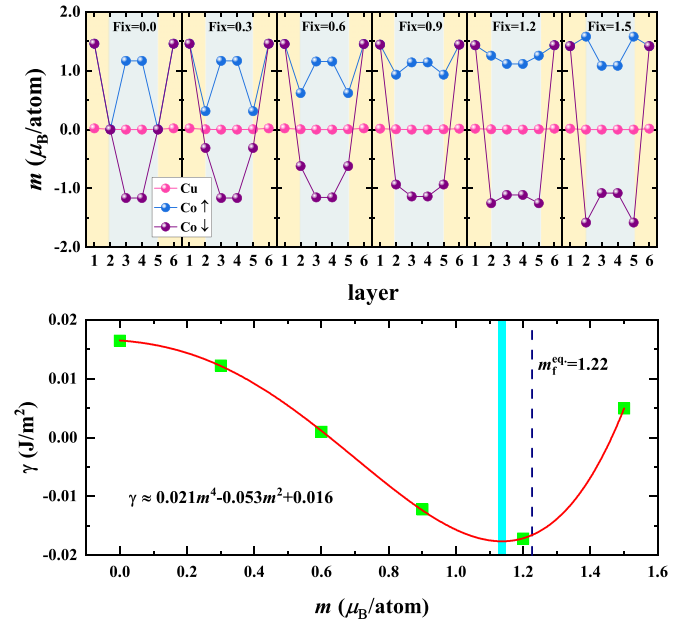

FIG. 5. Effect of local magnetic moments on the interfacial energy in the PM+FM/FM $Cu_{0.7}Co_{0.3}$/$Cu_{0.3}Co_{0.7}$ interface. The upper panel presents the magnetic moments on the Cu-rich side with respect to the size of the fixed spin for Co atoms in subinterface layers 2 and 5. The lower panel shows the interfacial energy as a function of the fixed spin. The solid line is the polynomial fit according to the Landau theory. The fully self-consistent equilibrium magnetic moment ($m_f^{eq.}$) is shown by the dashed line.

various kinetic models for precipitation nucleation and coarsening. In the early studies, Servi and Turnbull [18] measured the homogeneous nucleation kinetics of the Co-rich precipitate in the Cu-rich solid solutions, then they applied the classical homogeneous nucleation theory to their data and extracted an interfacial energy of ~0.2 J/m^2. Applying a similar method, Shiflet [58] obtained an interfacial energy of 0.165 J/m^2. It is important to note that the equation used by Servi and Turnbull, as well as by Shiflet, is essentially based on Becker's nearest neighbor broken bond model [22]. A critical assumption is that the two phases composed of the interface are homogeneous in composition right up to the boundary [58].

In the LSW theory of precipitation coarsening, the average radius of precipitate r increases with time t via

$$r^3 - r_0^3 = K(t - t_0) \qquad (3)$$

and

$$K = \frac{8D\gamma C_e V_m^2}{9RT} g(f), \qquad (4)$$

where r_0 is the average radius at the beginning of coarsening, K is a rate constant experimentally determined from the coarsening kinetics, $V_m = a_{Co}^3 N_A/4$ (N_A is the Avogadro's number) is the molar volume of fcc Co, D is diffusion coefficient of Co in Cu, C_e is the equilibrium concentration of Co in Cu, and $g(f)$ is correction prefactor for K for volume fraction f of the precipitate [7]. The interfacial energy reported by Oriani [57] varies significantly (0.1–0.9 J/m^2) in the temperature interval of 823–973 K using literature data

of precipitate size, D, and C_e, whereas $g(f)$ is not considered. Reassessment by Ardell [10] gave significantly smaller values of 0.18–0.32 J/m^2 when $g(f)$ was included. Watanabe [7] further criticized that the K values in the above studies were overestimated possibly because the precipitate radii were measured in the mixed stage of growth and coarsening. Using the revised K values, the interfacial energy obtained by Watanabe was 0.10–0.16 J/m^2. An independent application of the LSW theory yielded the interfacial energy of 0.15 J/m^2 in Cu-Co alloys containing 1–4 wt. % Co in the temperature span of 873–973K [7]. Watanabe *et al.* [21] further applied a coarsening theory developed by Kuehmann and Voorhees in Cu-Co alloys and derived the orientation-dependent interfacial energy. The (001) and (111) interfacial energies for the above mentioned alloys and temperatures are almost equal, being ~0.12 J/m^2. From the above experimental method for interfacial energy, we may notice several critical points. First, except for the complicated procedure in determining the interfacial energy, the experimental values vary significantly, highly dependent on many thermodynamic parameters and the kinetic models adopted. Second, sharp interface is assumed between the matrix of the equilibrium concentration and the precipitate of pure Co. Thereby, the experimentally determined interfacial energies at various temperatures actually correspond to interfaces with different compositions. The reported temperature dependence of the interfacial energy in the above studies is small over the studied temperature interval, which is consistent with the fact that the equilibrium concentration (C_e) of the matrix changes very little in the studied temperature interval of ~100 K according to the phase diagram [5].

B. Thermodynamic calculations of interfacial energy in Cu-Co alloys

In a phase separation system such as the fcc Cu-Co alloy here, the coherent interfacial energy γ between the two separating phases can be approximated by using Becker's sharp interface broken bond model [22,23]:

$$\gamma = \frac{Z_s N_s}{Z_l N_A} \Omega_{\text{Cu-Co}} \left(X_{\text{Co}}^{(\text{Cu})} - X_{\text{Co}}^{(\text{Co})} \right)^2. \tag{5}$$

Here Z_s is the number of cross bonds per atom at the interface, N_s is the number of atoms per unit area at the interface, Z_l is the coordination number of an atom within the bulk crystal lattice, N_A is the Avogadro's number, $\Omega_{\text{Cu-Co}}$ is the interaction energy of the fcc phase in the Cu-Co system, $X_{\text{Co}}^{(\text{Cu})}$ and $X_{\text{Co}}^{(\text{Co})}$ are the Co concentrations in the two separated fcc (Cu) and fcc (Co) phases, respectively. Nowadays, the interface energy and phase concentrations can be calculated on the basis of an available thermodynamic description for the Cu-Co system [60] by using a computational thermodynamic tool such as Thermo-Calc [61]. It is important to observe that the compositions of the precipitate/matrix interface ($X_{\text{Co}}^{(\text{Cu})}$ and $X_{\text{Co}}^{(\text{Co})}$) vary with temperature. Therefore, the calculated interfacial energy will vanish at the top of the miscibility gap where the concentrations of the matrix and precipitate are the same. This boundary condition applies also in the thermodynamic model for interfacial energy proposed by Kaptay [27], where he explicitly demonstrated that the
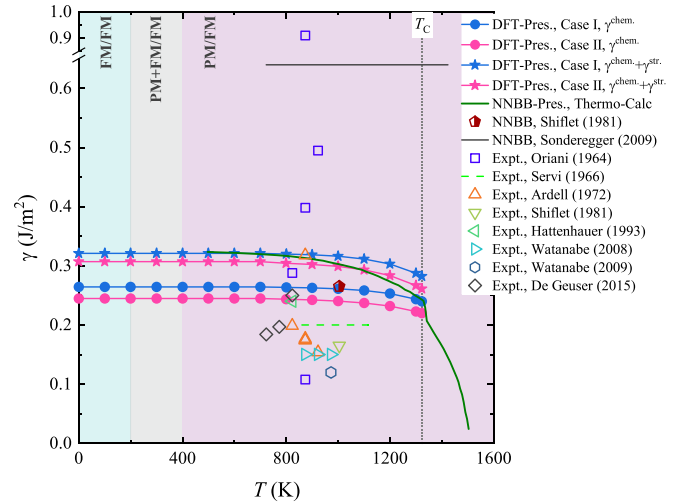

FIG. 6. The temperature dependence of the interfacial energy in fcc Cu-Co alloys obtained by *ab initio* calculations, thermodynamic NNBB models [23], and experiments [7,10,12,18,21,57–59]. The *ab initio* results calculated using the Cu-rich phase (case I) or the Co-rich phase (case II) as the underlying lattice are both shown (solid circles with lines), together with the results with additional contribution from strain energy (solid stars with lines).

interfacial energy decreases with increasing temperature and vanishes at the critical temperature of ~1100 K in the Au-Ni alloys. Furthermore, when applying the above thermodynamic models, the results are strongly dependent on thermodynamic parameters. For example, the coherent (111) interfacial energy was estimated to 0.265 J/m^2 at 1005 K in Cu-Co alloy by Shiflet using $\Omega = 33\,300$ J/mol [58]. While Sonderegger and Kozeschnik reported a value of 0.64 J/m^2 with no temperature dependence between 723 and 1423 K using different parameters [23]. Using Kubišta and Vřešt'ál's thermodynamic description [60], the temperature dependent interfacial energy calculated according to Eq. (5) is plotted in Fig. 6.

C. Translating composition dependence of interfacial energy to temperature dependence

For a coherent sharp interface with fixed composition on both sides, the temperature effects on the interfacial energy are expected from thermal lattice expansion, vibrational, magnetic, and electronic entropies. First-principles calculations may be used to estimate the above effects together with certain approximations like the quasiharmonic approximation and longitudinal spin fluctuations, etc. In the case of Ni/Ni$_3$Al coherent interfaces, Mao *et al.* showed that the above effects decrease the interfacial energies by ~15 mJ/m^2 from 0 to 1000 K [34]. Such calculations are very expensive, complicated, and time consuming, however, the final interfacial energies are only moderately affected. Additionally, it is even more challenging to perform such calculations for solid solutions and for magnetically disordered cases. Despite an accurate treatment of the temperature effects by the first-principles calculations may significantly improve our understanding of the temperature dependence of interfacial properties, currently such calculations are not feasible for the present case.

Here, as an effort to assess the size of the phonon contribution to the interfacial energy in Cu-Co alloys, we use two different supercells [6-Cu(111)/6-Co(111) and 9-Cu(111)/9-Co(111)] to estimate the energy vs volume and then derive the bulk moduli of the bulk (B_{bk}) and interface (B_i) regions, assuming that the supercells can be divided into interface [i.e., composed of 1-Cu(111)/1-Co(111)] and the rest bulk subsystems. Then the effect of phonons on the interfacial energy is assessed by $\Delta F^{ph} \approx F_i^{ph} - F_{bk}^{ph}$, where F_i^{ph} and F_{bk}^{ph} are the free energies of the interface and bulk subsystems as defined above. For two solids with similar Debye temperatures (Θ), one may estimate the free energy contribution (per atom) from phonons by $\Delta F^{ph} \approx 3k_B T(\Delta\Theta/\Theta)$ (valid at temperatures above the Debye temperature) [62]. Here the Debye temperatures for the bulk and interface subsystems are estimated from the bulk moduli obtained above, $\Theta \approx 67.48(rB/M)^{1/2}$, where r and M are the corresponding lattice parameter (in units of Bohr) and atomic mass. The bulk moduli for the interface and bulk subsystems are calculated to be 197.7 and 214.6 GPa, resulting Debye temperatures 618 and 644 K, respectively. Then we obtain $\Delta F^{ph} \approx -16.6$ meV/atom at 800 K, which corresponds to approx. -37 mJ/m^2 on the interfacial energy, considering that the interfacial subsystem is composed of two layers. This contribution is about 15% decrease of the 0 K interfacial energy (~ 250 mJ/m^2), similar to the results for the Ni/Ni$_3$Al interfaces [34] as well as the temperature effect on the surface energy of α Fe [63] based on *ab initio* phonon calculations.

Particularly, as implied by the above discussion on the experimental and thermodynamic interfacial energies of the matrix/precipitate interface in a specific alloy system, the temperature effects are primarily incorporated in the results through the changes of the equilibrium concentrations in the two phases. Therefore, in the following we try to correlate the composition dependence of the interfacial energy to temperature. The first step is to determine the equilibrium compositions of the matrix and the precipitate at various temperatures. One may use the experimental phase diagram to achieve this, or more interestingly, predict the equilibrium concentrations by the first-principles calculations. In our previous study we have successfully predicted the phase diagram for Cu-Co alloys using the first-principles calculations [5]. Starting from the Cu-Co phase diagram [5] and the composition dependent interfacial energies, we predict the interfacial energy as a function of temperature. The results are presented in Fig. 6 together with available results by experimental and thermodynamic calculations. With increasing temperature, the chemical interfacial energies for both cases I and II decrease with increasing temperature. Considering the large uncertainty of the experimental values, the *ab initio* and experimental results are comparable. Particularly, we are in a perfect agreement with the thermodynamic NNBB results regarding the temperature dependence below the Curie temperature (T_C) of Co. After adding the strain contribution estimated for a single layer of atoms, the agreement is further improved.

At T_C of Co, thermodynamic interfacial energy shows an abrupt drop of ~ 0.03 J/m^2. The slope of the interfacial energy above T_C is significantly larger than that below T_C. This is

likely due to the parametrization for the magnetic Gibbs free energy for the Co-rich phase [64]. To confirm this effect in first-principles calculations, we performed interfacial energy calculations for the PM Cu/PM Co interface using the experimental lattice constant of Co at T_C. The obtained interfacial energy is 0.262 J/m^2 for the PM/PM interface, in comparison to the 0.282 J/m^2 for the PM/FM interface. The difference of 0.02 J/m^2 is in good agreement with the decrease of thermodynamic results at T_C.

V. CONCLUSIONS

Ab initio calculations are expected to provide an alternative means to measure the interfacial energy between precipitate and matrix, besides the experimental methods and the thermodynamic calculations based on the NNBB models. The temperature dependence however have different focuses in these approaches, therefore it is critical to reach a better understanding in the values obtained from different approaches. In the present work we reviewed the experimental methods for estimating the interfacial energy based on kinetic models for precipitate nucleation and coarsening, as well as the thermodynamic models. We emphasized that the temperature effect on the interfacial energy of precipitate/matrix interface in such a system is primarily related to the change of the equilibrium compositions at varying temperatures. In contrast, the temperature effect of interfacial energy in *ab initio* calculations is usually related to the contributions from vibrational and magnetic entropies for an interface with fixed compositions. Therefore, for the purpose to use *ab initio* interfacial energies as input for computational modeling of precipitate nucleation and growth, and for understanding the observed precipitation and coarsening kinetics, the temperature dependent interfacial energy may be reformulated as a composition dependent quantity. In Cu-Co binary alloys, we calculated the magnetism and composition dependent interfacial energies, and translated the composition dependence to the temperature dependence. Our results show a reasonable agreement with both experimental and thermodynamic values. The present results and understanding are expected to improve the status of using *ab initio* interfacial energy in various thermodynamic and kinetic models.

ACKNOWLEDGMENTS

[1] L. Y. Chen, J. Q. Xu, H. Choi, H. Konishi, S. Jin, and X. C. Li, Rapid control of phase growth by nanoparticles, Nat. Commun. **5**, 3879 (2014).

[2] S. Liu, J. Jie, Z. Guo, S. Yue, and T. Li, A comprehensive investigation on microstructure and magnetic properties of immiscible Cu-Fe alloys with variation of Fe content, Mater. Chem. Phys. **238**, 121909 (2019).

[3] J. Z. Zhao and L. Ratke, A model describing the microstructure evolution during a cooling of immiscible alloys in the miscibility gap, Scr. Mater. **50**, 543 (2004).

[4] X. Fan, T. Mashimo, X. Huang, T. Kagayama, A. Chiba, K. Koyama, and M. Motokawa, Magnetic properties of Co-Cu metastable solid solution alloys, Phys. Rev. B **69**, 094432 (2004).

[5] C. Li, H. Levämäki, R. Xie, L. Tian, Z. Dong, W. Li, S. Lu, Q. Chen, J. Ågren, and L. Vitos, Critical assessment of Co-Cu phase diagram from first-principles calculations, Phys. Rev. B **102**, 184428 (2020).

[6] T. Miyazawa, Y. Ozawa, Y. Miyajima, T. Fujii, S. Onaka, and M. Kato, Morphological and crystallographic characteristics of incoherent octahedral fcc Co precipitates in a Cu matrix, Mater. Trans. **53**, 893 (2012).

[7] D. Watanabe, C. Watanabe, and R. Monzen, Coarsening behavior of Co precipitates in Cu-Co alloys, Metall. Mater. Trans. A **39**, 725 (2008).

[8] I. M. Lifshitz and V. V. Slyozov, The kinetics of precipitation from supersaturated solid solutions, J. Phys. Chem. Solids **19**, 35 (1961).

[9] C. Wagner, Theorie der alterung von niederschlägen durch umlösen (Ostwald-reifung), Z. Elektrochem. **65**, 581 (1961).

[10] A. J. Ardell, The effect of volume fraction on particle coarsening: theoretical considerations, Acta Metall. **20**, 61 (1972).

[11] R. Busch, F. Gärtner, C. Borchers, P. Haasen, and R. Bormann, High resolution microstructure analysis of the decomposition of Cu90Co10 alloys, Acta Mater. **44**, 2567 (1996).

[12] R. Hattenhauer and P. Haasen, The decomposition kinetics of Cu–1 at.% Co at 823 K, studied by bright-field-zone-axis-incidence transmission electron microscopy, Philos. Mag. A **68**, 1195 (1993).

[13] S. N. Zhevnenko and E. I. Gershman, Grain boundary phase transformation in Cu-Co solid solutions, J. Alloys Compd. **536**, S554 (2012).

[14] A. Bachmaier, M. Pfaff, M. Stolpe, H. Aboulfadl, and C. Motz, Phase separation of a supersaturated nanocrystalline Cu–Co alloy and its influence on thermal stability, Acta Mater. **96**, 269 (2015).

[15] S. Y. Hu, M. I. Baskes, M. Stan, and L. Q. Chen, Atomistic calculations of interfacial energies, nucleus shape and size of θ' precipitates in Al-Cu alloys, Acta Mater. **54**, 4699 (2006).

[16] A. J. Ardell and R. B. Nicholson, The coarsening of γ' in Ni-Al alloys, J. Phys. Chem. Solids **27**, 1793 (1966).

[17] J. D. Livingston, Critical particle size for precipitation hardening, Trans. Metall. Soc. AIME **215**, 566 (1959).

[18] I. S. Servi and D. Turnbull, Thermodynamics and kinetics of precipitation in the copper-cobalt system, Acta Metall. **14**, 161 (1966).

[19] D. Watanabe, K. Higashi, C. Watanabe, and R. Monzen, Ostwald ripening of Co particles in a Cu-1 mass% Co alloy, J. Jpn. Inst. Light Met. **71**, 151 (2007).

[20] D. Watanabe, C. Watanabe, and R. Monzen, Effect of coherency on coarsening of second-phase precipitates in Cu-base alloys, J. Mater. Sci. **43**, 3946 (2008).

[21] D. Watanabe, C. Watanabe, and R. Monzen, Determination of the interface energies of spherical, cuboidal and octahedral face-centered cubic precipitates in Cu–Co, Cu–Co–Fe and Cu–Fe alloys, Acta Mater. **57**, 1899 (2009).

[22] R. Becker, Die Keimbildung bei der Ausscheidung in metallischen Mischkristallen, Ann. Phys. **424**, 128 (1938).

[23] B. Sonderegger and E. Kozeschnik, Generalized nearest-neighbor broken-bond analysis of randomly oriented coherent interfaces in multicomponent fcc and bcc structures, Metall. Mater. Trans. A **40**, 499 (2009).

[24] Q. Chen, J. Jeppsson, and J. Ågren, Analytical treatment of diffusion during precipitate growth in multicomponent systems, Acta Mater. **56**, 1890 (2008).

[25] Q. Chen, K. Wu, G. Sterner, and P. Mason, Modeling precipitation kinetics during heat treatment with calphad-based tools, J. Mater. Eng. Perform. **23**, 4193 (2014).

[26] K. Wu, Q. Chen, and P. Mason, Simulation of precipitation kinetics with non-spherical particles, J. Phase Equilib. Diffus. **39**, 571 (2018).

[27] G. Kaptay, On the interfacial energy of coherent interfaces, Acta Mater. **60**, 6804 (2012).

[28] P. Hohenberg and W. Kohn, Inhomogeneous electron gas, Phys. Rev. **136**, B864 (1964).

[29] W. Kohn and L. J. Sham, Self-consistent equations including exchange and correlation effects, Phys. Rev. **140**, A1133 (1965).

[30] R. Benedek, A. Alavi, D. N. Seidman, L. H. Yang, D. A. Muller, and C. Woodward, First Principles Simulation of a Ceramic/Metal Interface with Misfit, Phys. Rev. Lett. **84**, 3362 (2000).

[31] S. Lu, Q. M. Hu, R. Yang, B. Johansson, and L. Vitos, First-principles determination of the α- α' interfacial energy in Fe-Cr alloys, Phys. Rev. B **82**, 195103 (2010).

[32] S. Lu, Q. M. Hu, M. P. J. Punkkinen, B. Johansson, and L. Vitos, First-principles study of fcc-Ag/bcc-Fe interfaces, Phys. Rev. B **87**, 224104 (2013).

[33] L. A. Zotti, S. Sanvito, and D. D. O'Regan, A simple descriptor for energetics at fcc-bcc metal interfaces, Mater. Des. **142**, 158 (2018).

[34] Z. Mao, C. Booth-Morrison, E. Plotnikov, and D. N. Seidman, Effects of temperature and ferromagnetism on the γ-Ni/γ'-Ni$_3$Al interfacial free energy from first principles calculations, J. Mater. Sci. **47**, 7653 (2012).

[35] R. Li, S. Lu, D. Kim, S. Schönecker, J. Zhao, S. K. Kwon, and L. Vitos, Stacking fault energy of face-centered cubic metals: Thermodynamic and ab initio approaches, J. Phys.: Condens. Matter **28**, 395001 (2016).

[36] S. Onaka, T. Fujii, and M. Kato, Elastic strain energy due to misfit strains in a polyhedral precipitate composed of low-index planes, Acta Mater. **55**, 669 (2007).

[37] H. Liu, I. Papadimitriou, F. X. Lin, and J. LLorca, Precipitation during high temperature aging of Al-Cu alloys: A multiscale analysis based on first principles calculations, Acta Mater. **167**, 121 (2019).

[38] L. Vitos, Total-energy method based on the exact muffin-tin orbitals theory, Phys. Rev. B **64**, 014107 (2001).

[39] L. Vitos, I. A. Abrikosov, and B. Johansson, Anisotropic Lattice Distortions in Random Alloys from First-Principles Theory, Phys. Rev. Lett. **87**, 156401 (2001).

[40] L. Vitos, H. L. Skriver, B. Johansson, and J. Kollár, Application of the exact muffin-tin orbitals theory: The spherical cell approximation, Comput. Mater. Sci. **18**, 24 (2000).

[41] J. P. Perdew and Y. Wang, Accurate and simple analytic representation of the electron-gas correlation energy, Phys. Rev. B **45**, 13244 (1992).

[42] J. P. Perdew, A. Ruzsinszky, G. I. Csonka, O. A. Vydrov, G. E. Scuseria, L. A. Constantin, X. Zhou, and K. Burke, Restoring the Density-Gradient Expansion for Exchange in Solids and Surfaces, Phys. Rev. Lett. **100**, 136406 (2008).

[43] L. Vitos, J. Kollár, and H. L. Skriver, Full charge-density calculation of the surface energy of metals, Phys. Rev. B **49**, 16694 (1994).

[44] L. Vitos, J. Kollár, and H. L. Skriver, *Ab initio* full charge-density study of the atomic volume of α-phase Fr, Ra, Ac, Th, Pa, U, Np, and Pu, Phys. Rev. B **55**, 4947 (1997).

[45] M. Asato, A. Settels, T. Hoshino, T. Asada, S. Blügel, R. Zeller, and P. H. Dederichs, Full-potential KKR calculations for metals and semiconductors, Phys. Rev. B **60**, 5202 (1999).

[46] H. Levämäki, M. P. J. Punkkinen, K. Kokko, and L. Vitos, Quasi-non-uniform gradient-level exchange-correlation approximation for metals and alloys, Phys. Rev. B **86**, 201104(R) (2012).

[47] H. Levämäki, M. P. J. Punkkinen, K. Kokko, and L. Vitos, Flexibility of the quasi-non-uniform exchange-correlation approximation, Phys. Rev. B **89**, 115107 (2014).

[48] B. L. Gyorffy, Coherent-potential approximation for a nonoverlapping-muffin-tin-potential model of random substitutional alloys, Phys. Rev. B **5**, 2382 (1972).

[49] F. Körmann, D. Ma, D. D. Belyea, M. S. Lucas, C. W. Miller, B. Grabowski, and M. H. F. Sluiter, "Treasure maps" for magnetic high-entropy-alloys from theory and experiment, Appl. Phys. Lett. **107**, 142404 (2015).

[50] When applying this approach to a "composite" like the present interfacial system, the paramagnetic-ferromagnetic energy differences should also be expressed per magnetic atoms involved in each magnetic transition process. For instance, when we compare the FM/FM and PM/FM cases for the 9+9 atoms supercell for the 10% alloy, the total number of magnetic atoms involved in the magnetic ordering is 9×0.1 (10% Co in the Cu-rich layers). Similarly, when we compare the FM/FM and PM+FM/FM cases (same supercell), only 7×0.1 magnetic atoms contribute to the magnetic ordering. Using the FM/FM, PM + FM/FM, PM/FM, and PM/PM energies, we finally ob-

[51] A. J. Pindor, J. Staunton, G. M. Stocks, and H. Winter, Disordered local moment state of magnetic transition metals: A self-consistent KKR CPA calculation, J. Phys. F **13**, 979 (1983).

[52] P. E. Blöchl, Projector augmented-wave method, Phys. Rev. B **50**, 17953 (1994).

[53] M. Ropo, K. Kokko, and L. Vitos, Assessing the Perdew-Burke-Ernzerhof exchange-correlation density functional revised for metallic bulk and surface systems, Phys. Rev. B **77**, 195445 (2008).

[54] Y. Kong and B. Liu, First-Principles Calculation of the structural, magnetic, and electronic properties of the Co_xCu_{1-x} solid solutions using special quasirandom structures, J. Phys. Soc. Jpn. **76**, 024605 (2007).

[55] R. E. Smallman and A. H. W. Ngan, Chapter 10. Surfaces, grain boundaries and interfaces, in *Modern Physical Metallurgy (Eighth Edition)*, edited by R. E. Smallman and A. H. W. Ngan (Butterworth-Heinemann, Oxford, 2014), pp. 415–442

[56] L. D. Landau and E. M. Lifshitz, *Course of Theoretical Physics, 3rd ed.* (Pergamon, Oxford, 1980), Vol. 5.

[57] R. A. Oriani, Ostwald ripening of precipitates in solid matrices, Acta Metall. **12**, 1399 (1964).

[58] G. J. Shiflet, Y. W. Lee, H. I. Aaronson, and K. C. Russell, A re-assessment of the comparison of classical homogeneous nucleation theory and experiment in Cu-Co alloys, Scr. Metall. **15**, 719 (1981).

[59] F. De Geuser, M. J. Styles, C. R. Hutchinson, and A. Deschamps, High-throughput in-situ characterization and modeling of precipitation kinetics in compositionally graded alloys, Acta Mater. **101**, 1 (2015).

[60] J. Kubišta and J. Vřešťál, Thermodynamics of the liquid Co-Cu system and calculation of phase diagram, J. Phase Equilib. **21**, 125 (2000).

[61] J. O. Andersson, T. Helander, L. Höglund, P. Shi, and B. Sundman, Thermo-Calc & DICTRA, computational tools for materials science, Calphad **26**, 273 (2002).

[62] G. Grimvall, Polymorphism of metals. III. Theory of the temperature-pressure phase diagram of iron, Phys. Scr. **13**, 59 (1976).

[63] S. Schönecker, X. Li, B. Johansson, S. K. Kwon, and L. Vitos, Thermal surface free energy and stress of iron, Sci. Rep. **5**, 1 (2015).

[64] M. Palumbo, S. Curiotto, and L. Battezzati, Thermodynamic analysis of the stable and metastable Co–Cu and Co–Cu–Fe phase diagrams, Calphad **30**, 171 (2006).

tain the critical temperatures around 200, 400, and 1100 K, respectively.